HAL
open science

Predicting the atmospheric carbonation of cementitious materials using fully coupled two-phase reactive transport modelling

Nicolas Seigneur, E. Kangni-Foli, Vincent Lagneau, A. Dauzères, Stéphane Poyet, P. Le Bescop, E L'Hôpital, Jean-Baptiste D'espinose de Lacaillerie

▶ To cite this version:

Nicolas Seigneur, E. Kangni-Foli, Vincent Lagneau, A. Dauzères, Stéphane Poyet, et al.. Predicting the atmospheric carbonation of cementitious materials using fully coupled two-phase reactive transport modelling. Cement and Concrete Research, 2020, 130, pp.105966. 10.1016/j.cemconres.2019.105966 . hal-02456212

HAL Id: hal-02456212

https://minesparis-psl.hal.science/hal-02456212

Submitted on 27 Jan 2020

HAL is a multi-disciplinary open access archive for the deposit and dissemination of scientific research documents, whether they are published or not. The documents may come from teaching and research institutions in France or abroad, or from public or private research centers.

L'archive ouverte pluridisciplinaire **HAL**, est destinée au dépôt et à la diffusion de documents scientifiques de niveau recherche, publiés ou non, émanant des établissements d'enseignement et de recherche français ou étrangers, des laboratoires publics ou privés.

Distributed under a Creative Commons Attribution - NonCommercial - NoDerivatives 4.0 International License

Predicting the atmospheric carbonation of cementitious materials using fully coupled two-phase reactive transport modelling

N. Seigneur[1], E. Kangni-Foli[2,3,4], V. Lagneau[1], A. Dauzères[2], S. Poyet[3], P. Le Bescop[3], E. L'Hôpital[2], J.-B. d'Espinose de Lacaillerie[4]

Abstract

The durability assessment of cementitious materials and concrete subjected to atmospheric carbonation of concrete has been an extensive study of research. Experimental studies on the subject show, among other results, that the response depends strongly on the cement composition. This paper focuses on two model materials: an hydrated C_3S paste and a low-pH paste, which exhibits a higher tendency to cracking. We show that a fully coupled reactive transport model can reproduce the measured experimental depths of carbonation without a need of fitting parameters. A sensitivity provides insights about the most relevant parameters to accurately model the atmospheric carbonation. Furthermore, results suggest that low-pH cement materials might be inherently less mechanically robust when subjected to atmospheric carbonation, due to a higher C-S-H decalcification rate. This implies that these materials are more likely to develop fractures, which could have implications in the framework of gas or radioactive waste disposal.

Keywords:
Atmospheric carbonation, Reactive Transport Modelling, Variable Porosity, Hytec, Chemistry and flow coupling, Multiphase flow

List of Symbols and Acronyms

γ_i	Activity coefficient of species i [-]
κ	Intrinsic permeability - [m^2]
$\mathcal{V}_j$	Molar volume of solid species j [$L.mol^{-1}$]

Email address: `nicolas.seigneur@mines-paristech.fr` (N. Seigneur)
[1]MINES ParisTech, PSL University, Centre de géosciences, 35 rue St Honoré, 77300 Fontainebleau, France.
[2]Institute for Radiological Protection and Nuclear Safety (IRSN)/PSE-ENV/SEDRE/LETIS, BP 17, 92262 Fontenay aux Roses, France.
[3]Den-Service d'Etude du Comporptement des Radionucléides (SECR), CEA, Université Paris-Saclay, F-91191 Gif-sur-Yvette, France.
[4]ESPCI Paris, PSL University, Soft Matter Science and Engineering, UMR CNRS 7615, 10 rue Vauquelin, 75005 Paris, France.

μ_α	Viscosity of fluid phase α [kg/m/s]
ω	Porosity [-]
$\overrightarrow{g}$	Gravitational acceleration vector (g is its norm) [m.s^{-2}]
$\overrightarrow{u_\alpha}$	Darcy-velocity of phase α [m.s^{-1}]
ρ_α	Density of phase α [kg.m^{-3}]
a_i	Activity of species i [-]
c_i	Molarity of species i [mol.L$^{-1}_{\text{water}}$]
D^α	Effective diffusion coefficient in phase α [m^2.s^{-1}], obtained through an empirical relation, such as Millington-Quirk
D_0^α	Intrinsic diffusion coefficient in phase α [m^2.s^{-1}]
K	Hydraulic conductivity - [m.s^{-1}]
K_j	Thermodyanmic equilibrium constant of the chemical reaction forming the secondary species j
$k_{r\alpha}$	Relative permeability of fluid phase α [-]
N_i	Total amount of basis species i [mol]
n_i	Number of moles of species i [mol]
p_c	Capillary pressure [Pa]
p_j	Partial pressure of gaseous species j [Pa]
p_α	Pressure of phase α [Pa]
R_α	Volumetric rate of phase α per unit of overall volume and time [s^{-1}]
R_i^α	Mass source term of species i in phase α [mol.s^{-1}]
S_α	Saturation of fluid phase α [-]
$S_{\alpha r}$	Residual saturation of phase α [-]
V_α	Volume of phase α in a node [m^3]
V_{tot}	Total volume of a node [m^3]
$\mathrm{a}_{(MQ)}$	Power of the porosity in the Millington-Quirk relation for the phase diffusion
$\mathrm{b}_{(MQ)}$	Power of the saturation in the Millington-Quirk relation for the phase diffusion
MIP	Mercury Intrusion Porosimetry
$\mathrm{n}^{(VG)}$	Power for the van Genuchten relations
$\mathrm{p}_e^{(VG)}$	Entry pressure for the van Genuchten relation of the capillary pressure [Pa]
REV	Representative Elementary Volume

1. Introduction

The carbonation of concrete and cementitious materials has always constituted a challenge from the modelling perspective. The carbonation process couples the dissolution of the calcium-bearing phases of the cement paste with the precipitation of different calcium carbonates. These reactions lead to significant modifications of the pore structure and pore size distribution [4, 5, 20], strongly impacting the flow and transport processes [1, 2, 3, 66]. For example, carbonation in saturated conditions can lead to the precipitation of an impermeable calcite layer on the material's surface [21, 28, 66], blocking any further transport processes through that layer. This is not always the case, as in different conditions, like high temperature and pressure conditions studied in [23, 24, 21], the carbonation depth can be much higher [10, 17, 18]. Furthermore, the composition of the cement paste can influence the carbonation [22]. Indeed, while a CEM I paste tends to see its porosity decrease during carbonation, other factors can lead to an increase of porosity, usually linked to the appearance of fractures [41, 59].

Carbonation alters the internal structure of the C-S-H through decalcification and silicates polymerisation reactions. This leads to volumetric variations [6, 7, 11], which induce tensile stress and potentially fractures [22, 38, 40]. Several studies have found that low-pH cement pastes tend to be more vulnerable to cracking during carbonation [8, 9, 40]. Depending on the experimental conditions and the material formulations, the effects of the carbonation can be quite different and challenging to interpret. Therefore, extensive studies of the carbonation processes are still on-going, both from a modelling and an experimental perspective (*e.g.* [15, 16]).

Cementitious materials are relevant to engineering projects such as radioactive waste management [28] and wells sealing in CO_2 storage [58]. In these contexts, carbonation occurs in unsaturated conditions. Thus, the different aforementionned phenomena are important to assess the durability of these materials. To this end, the atmospheric carbonation of cementitious materials has also been (and is still) extensively studied [12, 13, 14, 20, 38, 40]. Usually, as the atmospheric carbonation is a slow process ([54, 55]), accelerated carbonation has been considered experimentally. In most cases, this acceleration was achieved by increasing the partial pressure of CO_2. [32, 33, 34, 35, 36] have shown that the accelerated carbonation is still representative of natural carbonation for CO_2 partial pressures around below approximately 0.05 bar. Therefore, it is likely that a modelling approach able to predict the effects of an accelerated carbonation could be extended to any CO_2 conditions.

For that purpose, a complete and accurate understanding of the involved phenomena requires a full coupling between the chemical, thermal, mechanical and hydrological effects. In a nutshell, the main processes involved are:

- CO_2 gas transport;
- CO_2 dissolution in the pore water (which consumes water and acidifies the solution $CO_2(g) + H_2O \leftrightharpoons H_2CO_3$);
- dissolution and decalcification of hydrated minerals, which induces water release/consumption and shrinkage;
- calcium carbonates precipitation due to the reaction between dissolved CO_2 and aqueous calcium;

- shift in the pore size distribution of the material;
- modification of porosity and saturation through the evolution of solid minerals and water production/consumption, which have an impact on the fluids pressure.

One can understand that all of these processes impact one another: thus, it is a strongly coupled and nonlinear problem.

Reactive transport modelling is a natural tool to investigate the thermal, hydrodynamic and chemical coupling effects of the carbonation processes in unsaturated conditions. However, coupling reactive transport with mechanics is still pretty limited, for the main reason that the relevant chemical and mechanical processes operate on different scales, which would not be accounted for by a single representative elementary volume.

This study focuses on two similar model materials which exhibit quite different mechanical responses under atmospheric carbonation. On the one hand, we study a model hydrated C_3S paste which does not exhibit significant mechanical damage during carbonation. On the other hand, a similar low-pH material, which exhibits stronger mechanical damage is considered. The objectives of this study are twofold. First, the tool developed in [30] will be used to demonstrate its applicability and validity to model atmospheric carbonation of cementitious materials, as long as the associated mechanical damage are limited. This will, *in fine*, help modelling those types of reactions and hence improve the durability assessments. Second, the same tool will be used to try to provide an explanation for the different mechanical responses observed in ordinary and low-pH cements. In the end, this paper proposes different key experiments which could be performed to validate or refute the suggested explanation.

Section 2 briefly presents the experimental results on which the modelling study will be based, including the description of the experiments and the characterizations of the sound and carbonated model C_3S pastes. Section 3 is dedicated to the numerical simulations: it briefly describes the mathematical formulation of the reactive transport model, provides results of the simulations on the two materials as well as a sensitivity analysis. An extensive discussion is given in 4 which focuses on understanding why different materials behave differently. Section 5 summarizes and gives some perspectives to this work.

2. Summary of the experimental results

This section constitutes a brief description of the experimental results relevant to this work. More informations can be found in [70], [71] and [75].

2.1. Sound materials

Two pastes are here considered whose main properties relevant for the modelling are summarized in table 1. After fabrication, these two samples were kept for one month in their sealed moulds at ambient temperature, before being cured for two months in an equilibrium solution. More details about their manufactures, curing conditions and their characterizations can be found in [70]. The low-pH paste considered in this modelling study has a Ca/Si ratio of 1.4 and is made of C-S-H, with small traces of portlandite [75], which were not included in the model. This is likely due to chemical heterogeneity within the paste. The choice to focus on the latter for the modelling study (and not the

Table 1: Experimental value of the most relevant parameters to describe the sound samples (VF stands for volume fraction). See [70], [71] and [75] for more informations.

Label	**Porosity**	**Water-content**	**Porlandite**	**Effective gas diffusion**
C_3S	0.4	0.12	24% VF	1-1.5 $\times$ 10^{-7} m^2.s−1
Low-pH	0.56	0.166	0	Not measured

ones with lower Ca/Si ratios) was motivated by the fact that it is the closest from the hydrated C_3S paste (in terms of pH and C-S-H structure). This study aims at showing and understanding why these two rather similar materials exhibit different behaviors in the same experimental conditions. Samples are cylindrical (diameter $\phi = 30$ mm, height h = 110 mm).

Samples were set in a climatic chamber (initially without CO_2) prior to carbonation at a 25°C and 55% RH. The effective oxygen gas diffusion was measured to be between 1-1.5 $\times$ 10^{-7} m^2/s for the C_3S paste. These values are comparable to [73]. These values will be used to compute the effective CO_2 diffusion at a liquid saturation of 30% (similar for the two materials).

Mercury intrusion porosimetry was used to assess the pore (entry) size distribution of the different pastes (depicted in figure 1). Before MIP, samples were crushed, immersed for seven days in liquid nitrogen before being frozen-dried for 24 hours. These analysis do not aim to be quantitative but mainly indicate a shift in the pore size distributions towards smaller pores for the low-pH paste, even though total porosity is higher for the low-pH paste. This effect is expected as the pozzolanic reactions generate additional C-S-H. Additionally, the lower-radius mode is very close for both pastes, indicating similar C-S-H structure.

2.2. Carbonated materials

The carbonation process was initialized by maintaining a constant CO_2 partial pressure (respectively 0.0004 and 0.03 bar for natural and accelerated carbonation) in the climatic chamber while maintaining a 55% RH, using a saturated solution of $Mg(NO_3)_2$. As the material is in hydric equilibrium prior to the CO_2 injection, the initial migration of CO_2 is purely diffusive. At given times, samples were taken out of the carbonation chamber. These samples were cut in two parts; one half was stained with phenolphthalein to measure the carbonated depth and the other one was used to characterize the change in mineralogy.

More details about the carbonation depths measurements can be found in [71], but most important results for the modelling study are summarized in table 2. The uncertainty in the carbonation depth arises from the multiple characterization of the latter (X-Ray diffraction, μCT scan and phenolphtaleine).

One can observe a larger carbonation depth obtained for the low-pH paste. Additionnally, μCT scans (figure 2) show the development of fractures after 28 and 38 days of accelerated carbonation, respectively for the low-pH and C_3S samples. One can observe a higher crack-density for the low-pH sample.

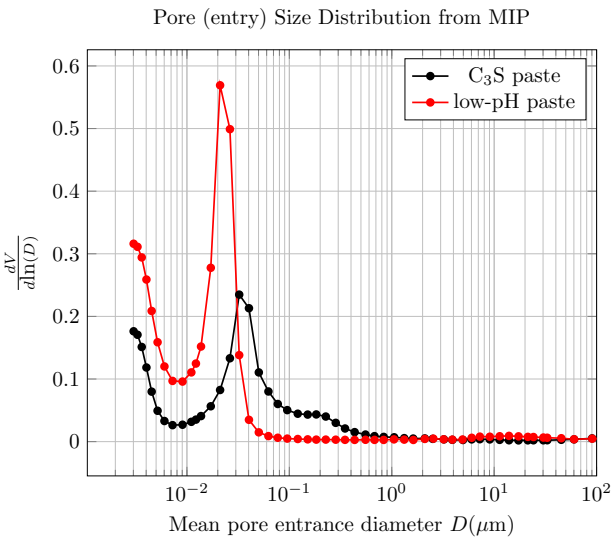

Figure 1: Representation of the pore size distributions of the two samples obtained by MIP, indicating a finer porosity for the low-pH paste.

Table 2: Characterization of the carbonated samples. The carbonation depth corresponds to the extent of the portlandite depleted zone. The uncertainty associated with the depth is the result of a combination of techniques, mainly XRD profiles, μCT scan, thermogravimetric analysis and phenolphtaleine tests.

Label	**Sample time (days)**	**Carbonation depth (mm)**
C_3S	38	6-8
	81	10-12
Low-pH	28	11-12
	71	17-19

3. Reactive transport modelling

3.1. Mathematical formulation

We hereby recall the main relevant equations which are going to be solved to model the fully coupled problem. For more informations, [30] describes in details the different approaches to this problem and how it is solved numerically.

3.1.1. Reactive system

Reactive set. The reactive system involves the different geochemical reactions representing the gas-liquid-solid system. These constitute a set of N_r geochemical reactions between N_s chemical species (N_{min} of which are mineral, N_{aq} are aqueous and N_g are gaseous). Hence it is possible to chose a set of N_b basis species C (denoted by the subscript i) upon which N_d other species S (referred to as secondary, denoted by the subscript j) can be defined:

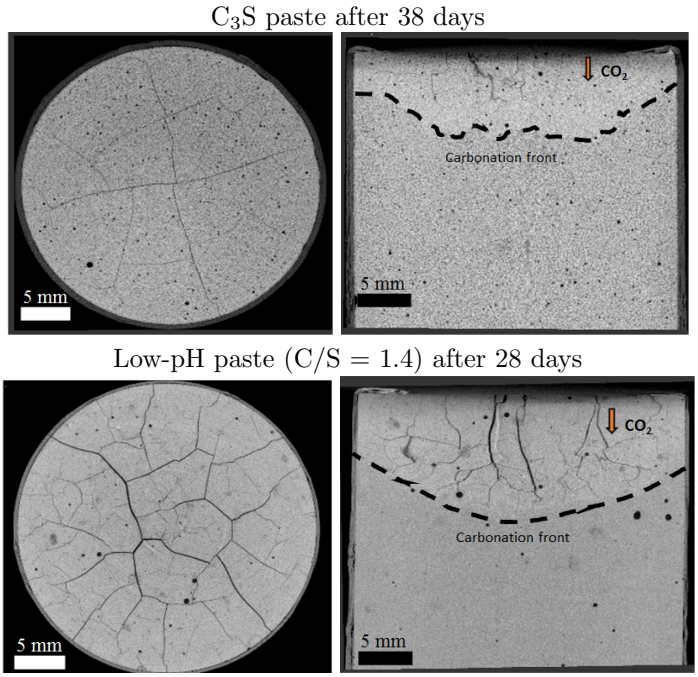

Figure 2: μCT scan of samples subjected to accelerated carbonation (voxel size = 17 μm). Left panel: top view of the sample, right panel: transverse view of the sample. These scans show the evolution of the carbonation front as well as the appearance of cracks. Measurement of the extent of the carbonation front were coupled with XRD profiles, thermogravimetric analysis and phenolphtaleine tests.

$$S_j \leftrightharpoons \sum_{i=1}^{N_b} \alpha_{ij} C_i. \tag{1}$$

This corresponds to the formalism of the primary and secondary species [49]. The resolution of the complete solid/gas/liquid equilibrium is based on a mass conservation. The total amount (in moles) of any primary species in all different phases has to be conserved. Solving the system of mass conservation equations for the amount (in moles) of each primary species (including water) allows to compute the evolution of all the other species, as well as the evolution of porosity and saturation.

The relationship between the activities of the secondary species (a_j) and basis species (a_i) use the Mass Action Law formalism transformed in terms of moles instead of concentrations:

$$n_j = m_{\mathrm{H_2O}} \frac{K_j}{\gamma_j} \prod_{i=1}^{N_b} (a_i)^{\alpha_{ij}}. \tag{2}$$

The activity of aqueous species is usually given by their concentrations (in molal) multiplied by an activity coefficient γ_i, computed using different empirical models (Debye-Huckel [51], b-dot [69], ...):

$$a_i = \gamma_i \frac{n_i}{m_{\mathrm{H_2O}}} \quad \text{if species } i \text{ is aqueous.} \tag{3}$$

The water activity is usually computed using Helgeson's model [68]. For the liquid-gas equilibrium $\mathrm{S_j(g)} \leftrightharpoons \mathrm{S_j(aq)}$, Henry's law relates the activity a_j of the aqueous species $\mathrm{S}_j\mathrm{(aq)}$ to the fugacity f_j of gaseous species $\mathrm{S}_j\mathrm{(g)}$ at equilibrium through Henry's constant H_j. Using the Mass Action Law for $a_{\mathrm{S_j(aq)}}$ and the ideal gas law to link the amount of gaseous to the volume and pressure of the gas phase, we can thus write a similar relationship to compute the amount of a gaseous species.

For solid and mineral phases, the Mass Action Law is also valid: their activities can be chosen as one for pure phase or can be computed using mixing rules for solid solutions. In this case, minerals will be considered at the thermodynamic equilibrium.

The resulting equations build a system of N_b equations which has the amount (in moles) of each N_b basis species as unknowns (n_i):

$$\begin{aligned}
&\forall\, i < N_b : \; N_i = n_i + \textstyle\sum_{j=1}^{N_d} \alpha_{ij} n_j \\
&\text{with } n_j = \begin{cases} m_{\mathrm{H_2O}} \dfrac{K_j}{\gamma_j} \displaystyle\prod_{i=1}^{N_b} (a_i)^{\alpha_{ij}} & \text{if species } j \text{ is aqueous} \\ \dfrac{H_j V_g}{RT} K_j \displaystyle\prod_{i=1}^{N_b} (a_i)^{\alpha_{ij}} & \text{if species } j \text{ is gaseous} \end{cases}, \\
&\text{with } a_i = \begin{cases} \dfrac{n_i \gamma_i}{m_{\mathrm{H_2O}}} & \text{if species } i \text{ is aqueous} \\ 1 & \text{otherwise} \end{cases},
\end{aligned} \tag{4}$$

3.1.2. Two-phase reactive transport

The reactive transport problem considers the transport in the gaseous and aqueous phase of the different mobile species. As gaseous and aqueous transport might be significantly different, the equations are written specifically for each fluid phase. The total amount in moles defined in chemistry corresponds to the total mobile, gaseous and immobile part of each basis species:

$$N_i = n_i^l + n_i^g + n_i^s, \tag{5}$$

where the transport (diffusive and advective) only operates on the mobile amounts, hence not on n_i^s. The geochemical liquid/solid/gas equilibrium is taken into account through source-terms R_i^g and R_i^s, describing the dissolution, evaporation, precipitation and sorption processes:

$$\begin{cases} \dfrac{1}{V_{\mathrm{tot}}} \dfrac{\partial n_i^l}{\partial t} = \mathrm{div}\left(D^l(\omega, S_l) \overrightarrow{\nabla} c_i - c_i \overrightarrow{u_l} \right) - \dfrac{R_i^s + R_i^g}{V_{\mathrm{tot}}} & \text{Aqueous} \\ \dfrac{1}{V_{\mathrm{tot}}} \dfrac{\partial n_i^g}{\partial t} = \mathrm{div}\left(D^g(\omega, S_g) \overrightarrow{\nabla} g_i - g_i \overrightarrow{u_g} \right) + \dfrac{R_i^g}{V_{\mathrm{tot}}} & \text{Gaseous} \end{cases} \tag{6}$$

where the source terms are defined as:

$$\begin{aligned} R_i^g &= \textstyle\sum_{j=1}^{\mathrm{N_g}} \alpha_{ij} \frac{\mathrm{d}n_j^g}{\mathrm{d}t} \\ R_i^s &= \textstyle\sum_{j=1}^{\mathrm{N_{min}}} \alpha_{ij} \frac{\mathrm{d}n_j^s}{\mathrm{d}t} \end{aligned}, \tag{7}$$

and where the concentrations (in moles per unit of volume) are defined as:

$$c_i = \frac{n_i}{V_{\mathrm{H_2O}}} \quad \text{and} \quad g_i = \frac{n_i^g}{V_g} \ . \tag{8}$$

Finally, the solid, liquid and gas volume are computed through the porosity ω, liquid saturation S_l and gas saturation S_g, which are given by:

$$\begin{cases} \omega = 1 - \dfrac{1}{V_{\mathrm{tot}}} \displaystyle\sum_{j=1}^{\mathrm{N_{min}}} n_j \mathcal{V}_j & \Longrightarrow \quad V_{\mathrm{solid}} = (1-\omega) V_{\mathrm{tot}} \\ S_l = \dfrac{n_{\mathrm{H_2O}} \mathcal{V}_l}{\omega V_{\mathrm{tot}}} & \Longrightarrow \quad V_{\mathrm{H_2O}} = \omega S_l V_{\mathrm{tot}} \\ S_g = 1 - S_l & \Longrightarrow \quad V_g = \omega S_g V_{\mathrm{tot}} \end{cases} \tag{9}$$

These last physical parameters have an influence on the transport properties: the diffusion coefficient for both fluid phase might evolve due to the geochemical reactions (porosity and saturation modifications).

The advective flux, arising from pressure and gravity gradients, is related to the Darcy-velocity $\overrightarrow{u_\alpha}$ which is provided by the compressible two-phase flow calculation, described in details in [42] and developed in [30], here presented without the gravity-terms:

$$\begin{cases} \dfrac{\partial \omega}{\partial t} = R_s \\ \dfrac{\partial \omega (1-S_g)\rho_l}{\partial t} = \overrightarrow{\nabla} \dfrac{\rho_l k_{rl} \kappa}{\mu_l} \overrightarrow{\nabla} p_l + \rho_l R_l \\ \dfrac{\partial \omega S_g \rho_g}{\partial t} = \overrightarrow{\nabla} \dfrac{\rho_g k_{rg} \kappa}{\mu_g} \overrightarrow{\nabla} (p_l + p_c) + \rho^g R_g \end{cases} \ . \tag{10}$$

For a fully coupled problem, the geochemical reactions which produce/consume water and solid phase, the reactive transport has an impact on flow which will be described by source terms for each phase:

$$\begin{cases} R_s = -\frac{\mathrm{d}\omega}{\mathrm{d}t} \\ R_l = \frac{1}{V_{\mathrm{tot}}} \frac{\mathrm{d}V_l}{\mathrm{d}t} \\ R_g = \frac{1}{V_{\mathrm{tot}}} \frac{\mathrm{d}V_g}{\mathrm{d}t} \end{cases} \ . \tag{11}$$

This problem will be solved using the reactive transport code Hytec [44, 47, 48, 57, 58, 46], which was extensively used and validated in numerous applications. The adopted resolution approach is the one described in [30].

3.2. Description of the simulations

This section focuses on the description of the simulation of the one-dimensional accelerated atmospheric carbonation of concrete. The simulation describes the carbonation from one side of a 5 cm initially partially saturated cementitious materials (2 mm grid size). The initial physical and geochemical conditions are uniform and representative of the experimental results, *i.e.* a 40% porosity with a 30% saturation, with an inert gas atmosphere.

3.2.1. Thermodynamic database

The considered aqueous, gaseous and mineral species, as well as their properties are given in tables 3, 4 and 5, gathering informations from the Thermoddem database [74]. If thermodynamic equilibrium is assumed, different calcium carbonates polymorphs cannot coexist. Reproducing the different calcium carbonates precipitation would therefore require a kinetic approach to the calcite precipitation. But, providing a kinetic formulation requires the definition of kinetic rate constants for each of the polymorph. Moreover, the origin of the precipitation of these different polymorphs seems to be different: aragonite and vaterite are typical when considering carbonation of C-S-H [38, 39]. These effects are not easily represented in a continuum approach.

Furthermore, Rietveld analysis shows that portlandite depletion is not complete. This cannot be represented by a model consisting of thermodynamic equilbrium for the mineral phases. Some authors suggested that the portlandite dissolution can be inhibited due the precipitation of a calcite coating on the surface of portlandite grains [53]. This could be taken into account through a kinetic dissolution of portlandite, *e.g.* using a Monod-type inhibition depending on calcite dissolution. Or using an accurate available surface model of the portlandite grains, which would be dependent on calcite volume fractions, similar to what has been described in [76, 77, 78, 67].

While these features could be modelled in a simulation, they would require several additional fitting parameters. We shall therefore assume only one calcium carbonate mineral species, namely calcite, modelled at equilibrium to reproduce the effect of the total calcium carbonate precipitation. Similarly, portlandite dissolution and C-S-H decalcification are modeled at equilibrium, an approach which was successful for cementitious materials [57]. As it will be witnessed, these assumptions lead to a pretty good match between simulated and measured carbonation depths, despite being an approximation of the chemical processes.

Table 3: Primary species considered in the model.

Name	Molar mass (g.mol^{-1})
H_2O	18.0153
H^+	1.0079
Ca^{2+}	40.0078
HCO_3^-	61.0171
H_4SiO_4	96.11486

3.2.2. Initial and boundary conditions

Initially, the geochemistry of the cementitious material, which is considered at equilibrium with Portlandite and CSH(1.6), is given in table 6. The initial volume fractions of portlandite and CSH(1.6) respectively are 24 and 36% (and the remaining 40% is porosity).

This material is set in contact with an atmosphere, represented by an atmospheric boundary conditions, in which the CO_2 partial pressure is set to 30 mbar. The density of the gas phase is assumed constant and independent of its composition. As the modelled

Table 4: Mineral database describing the mineral phases considered in the model and their respective relevant properties

Mineral	Composition	LogK	$\mathcal{V}$ ($cm^3.mol^{-1}$)
Portlandite	Ca^{2+} + 2 (H_2O - H^+)	-22.812	33.056
Calcite	Ca^{2+} + HCO_3^- - H^+	-1.8487	36.9339
CSH(1.6)	1.6 Ca^{2+} + H_4SiO_4 + 2.18 H_2O - 3.2 H^+	-28.002	84.68
CSH(1.2)	1.2 Ca^{2+} + H_4SiO_4 + 1.26 H_2O - 2.4 H^+	-19.301	71.9501
CSH(0.8)	0.8 Ca^{2+} + H_4SiO_4 + 0.34 H_2O - 1.6 H^+	-11.05	59.29
Am Silica	H_4SiO_4 - 2 H_2O	2.702	29

Table 5: Thermodynamic database of the gaseous and secondary aqueous species considered for the reactive transport problem.

Name	Composition	LogK
$CaOH^+$	Ca^{2+} + H_2O - H^+	-12.85
$CO_3^=$	HCO_3^- - H^+	-10.3288
H_2CO_3	HCO_3^- + H^+	6.3447
CO_2(g)	HCO_3^- + H^+ - H_2O	7.811
$CaCO_3$(aq)	Ca^{2+} + HCO_3^- - H^+	-7.0017
$CaHCO_3^+$	Ca^{2+} + HCO_3^-	1.0467
OH^-	H_2O - H^+	-13.9951
$HSiO3^-$	H_4SiO_4 - H_2O- H^+	-9.819
$H_2SiO_4^=$	H_4SiO_4 - 2 H^+	-23.27

processes are mostly driven by diffusion, this assumption does not have a significant impact on the simulation results.

3.2.3. Physical relations and parameters

The effective diffusion coefficient of the cementitious materials is supposed to evolve following a Millington-Quirk relationship:

$$D_\alpha(\omega, S_\alpha) = D_{0,\alpha} \left(\frac{\omega}{\omega_0}\right)^{a_{(MQ)}} \left(\frac{S_\alpha}{S_{0,\alpha}}\right)^{b_{(MQ)}}, \tag{12}$$

where ω_0 and $S_{0,\alpha}$ respectively represent the initial value of the porosity and saturation of phase α.

However, as this material has the same porosity and mineralogy as the one studied in [19], the effective diffusion coefficient in saturated condition is 2×10^{-11} m^2/s, and the porosity power is chosen to be 2, following the study of the carbonation in [66]. [60] suggests values of 2 and 4.2 respectively for the porosity and saturation exponents.

In the simulation, gas diffusion was computed using $D_{0,g} = 2.25\times10^{-7}$ m^2/s at a 30% saturation (70% gas-saturation), which is slightly more important than the measured value (1-1.5 $\times10^{-7}$ m^2/s). This parameter was slightly increased to match exper-

Table 6: Initial aqueous conditions for the reactive transport simulations

Component	Constraint	Value (C_3S)	Value (low-pH)	Unit
H_2O	Liquid Saturation S^l	0.3	0.3	-
H^+	pH	12.5	12.4	-
Ca^{2+}	Total concentration	21.09	1.94	mmolal
HCO_3^-	Total concentration	0	0	mmolal
H_4SiO_4	Total concentration	2.078	77.7	μmolal

imental carbonation profiles. This slight increase could potentially be explained by the appearance of cracks in the carbonated zone.

This rather important value for the gas diffusion limits the simulation timestep. For a spatial resolution of 2 mm, the timestep should not be higher than 10 seconds.

The intrinsic permeability of the material is assumed to be close than the one computed in [40], *i.e.* 2.7× 10^{-22} m^2. As water is not going to flow away of the material, the intrinsic relative permeability of the atmospheric cell is set very small (10^{-6}) (representative of a no-flux boundary condition). Besides that, the relative permeabilities and the capillary pressure are computed based on the van Genuchten relations:

$$p_c(S^l) = p_e^{(VG)} \left(\left(\frac{1 - S^l - S_r^l}{1 - S_r^l - S_r^g} \right)^{-1/n^{(VG)}} \right)^{1-n^{(VG)}} \tag{13}$$

$$k_{rg}(S^g) = \sqrt{\frac{S^g - S_r^g}{1 - S_r^l - S_r^g}} \left(1 - \left(\frac{S^g - S_r^g}{1 - S_r^l - S_r^g} \right)^{1/n^{(VG)}} \right)^{2n^{(VG)}} \tag{14}$$

$$k_{rl}(S^l) = \sqrt{\frac{S^l - S_r^l}{1 - S_r^l - S_r^g}} \left(1 - \left(\frac{S^l - S_r^l}{1 - S_r^l - S_r^g} \right)^{1/n^{(VG)}} \right)^{2n^{(VG)}} . \tag{15}$$

3.3. Simulation of the atmospheric carbonation of the C3S paste

3.3.1. Reference case

The results of the accelerated carbonation of the C_3S paste are represented in figures 3, 4 and 5 (which represents most hydrodynamic parameters). Figure 3 shows the progressive dissolution of the portlandite and decalcification of the C-S-H structure parallel to the calcite precipitation. One can notice the in-depth carbonation of portlandite.

The temporal evolution of the mineralogical profile in the first two milimeters of cement is depicted in figure 4. It shows the typical mineralogical evolution of the different mineralogical phase: it takes less than 4 days to completely consume portlandite within the first two milimeters of cement. After the portlandite dissolution, a second type of C-S-H precipitates and the decalcification of the C-S-H starts. Simulation predicts the formation of a silica gel phase after only 7 days.

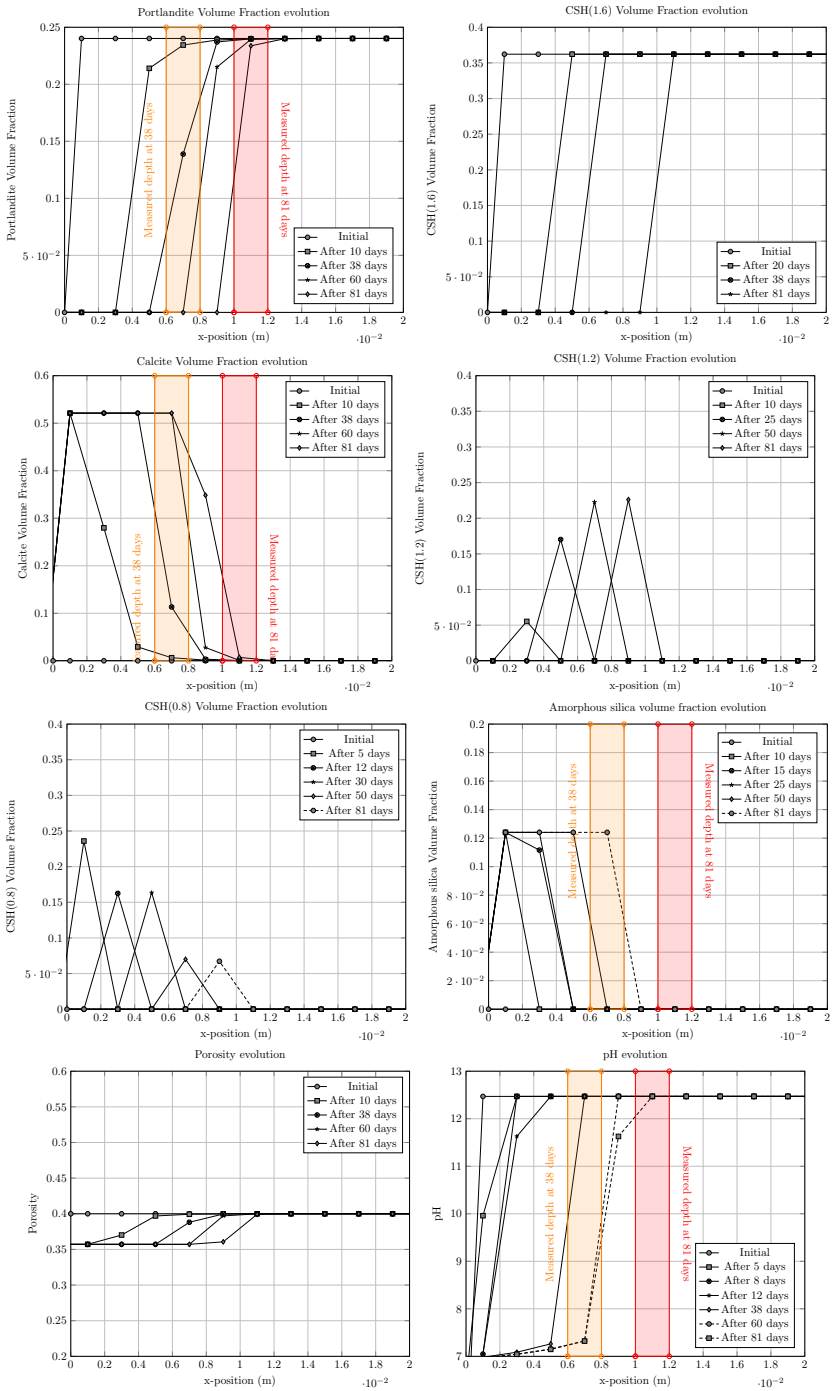

Figure 3: Evolution of the mineral, porosity and pH profiles during accelerated carbonation of the C_3S sample. Highlighted carbonated regions in orange and red correspond to the experimental measurements of the carbonation depths summed up in table 2

Table 7: Physical parameters values required for the reactive transport simulations.

Parameter	Value	Unit
$D_{0,l}$	2×10^{-11}	$m^2.s^{-1}$
$D_{0,g}$	2.25×10^{-7}	$m^2.s^{-1}$
$a_{(MQ)}$	2	-
$b_{(MQ)}$	4.2	-
κ	2.7×10^{-22}	m^2
μ_l	8.9×10^{-4}	$kg.m^{-1}.s^{-1}$
μ_g	1.78×10^{-5}	$kg.m^{-1}.s^{-1}$
ρ_l	997	$kg.m^{-3}$
ρ_g	1.13	$kg.m^{-3}$
$n^{(VG)}$	0.481	-
S_r^{α}	0.01	-
$p_e^{(VG)}$	10	kPa

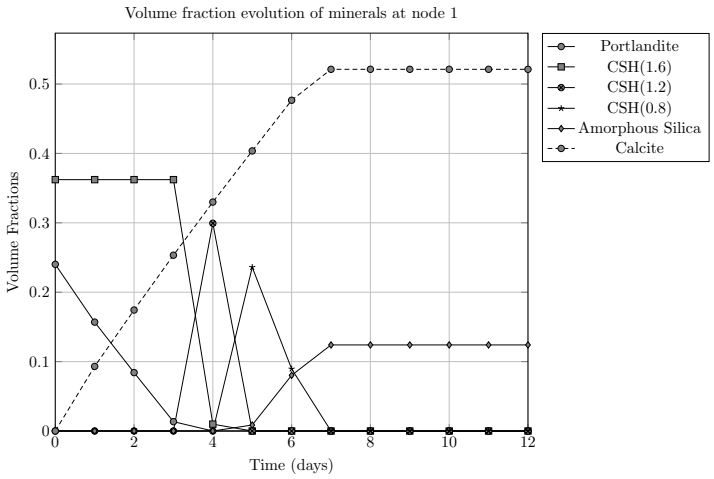

Figure 4: Evolution of mineralogy in the first two milimeters of the C_3S paste over time

The modelled system is fully coupled, meaning that chemical reactions are coupled to the two-phase flow. Figure 5 summarizes the hydrodynamic behavior of the system. It describes how the different geochemical processes induce gas and liquid advection. While the inert gases diffuse towards the atmosphere, this is compensated by the diffusion of CO_2 within the material. But, as most of it dissolves in water (see top right graph of figure 5), this leads to a decrease in gas-pressure in the material and creates a slow gas advective flux.

Liquid water is not allowed out of the material: a no-flow boundary condition is consistent with a partially-saturated porous medium in contact with atmosphere. However, the local increase in fluid pressures induced by the chemical reaction induces a (very

Table 8: Summary of the additional simulations. When the affected parameter have an influence on another one (example, higher porosity for the low-pH formulation), other parameters were changed accordingly to match the reference simulation.

Label	Parameter	Reference Value	New value	Unit
High permeability	κ	2.7×10^{-22}	2.7×10^{-19}	m^2
High Gas diffusion	$D_{0,g}$	2.25×10^{-7}	4.5×10^{-7}	$m^2.s^{-1}$
Low Gas diffusion	$D_{0,g}$	2.25×10^{-7}	1×10^{-7}	$m^2.s^{-1}$
High aqueous diffusion	D_0, l	2×10^{-11}	2×10^{-10}	$m^2.s^{-1}$
High water-content	$S^l(t=0)$	0.3	0.4	-
Low p_{CO_2}	p_{CO_2}	0.03	0.003	bar

slow) liquid advection inside the material. The evolution of the mass of water, resulting from the flow and the goechemical reactions is also given. The different geochemical reactions globally lead to a local decrease in water content. While this might be surprising, as portlandite dissolution and decalcification release water, an important mass of water is consumed due to the dissolution of CO_2(g). As the water mass slightly decreases, as porosity, liquid saturation remains rather constant. The applicability of this modelling to an advective problem is possible, but the different unsaturated laws and parameters should be precisely determined.

The simulated values are pretty close to the measured ones. The portlandite dissolution extent is respectively 7 and 10 mm after respectively 38 and 81 days, while the pH modification is slightly delayed from the decalcification of the C-S-H phase. We want to emphasize that this simulation describes accurately the different relevant coupled processes involved in the carbonation, and every input parameters were obtained experimentally or are close to usually accepted values. There were no fitting parameters involved. This shows the physical reliability of the provided modelling. We suggest to perform a deeper analysis on the aforementioned parameters through a sensitivity analysis, which will study how the relevant parameters will impact the global results.

3.3.2. Sensitivity Analysis

Based on the previous results, we will investigate how the simulation results are impacted by modifying some of the input parameter. Therefore, a few cases are investigated, depending on how likely these parameters have a strong influence on modelling results and how much uncertainty there is in their measurements (higher permeability, different diffusion, various CO_2 partial pressure, higher water-contents). Table 8 describes the different investigated cases and defines the modified parameter and the label associated with every one of these simulations.

The results are presented in figure 6 and focus on the evolutions of the portlandite, calcite and porosity profiles after 60 days of low p_{CO_2} (yet higher than atmospheric) carbonation. One can see that the effect of the aqueous diffusion or permeability is very limited. This indicates that carbonation is mostly driven by CO_2 diffusion, as predicted in [63]. This is confirmed by the results of the sensitivity analysis for the lower and high gas diffusion. Also, a higher water-content leads to a lower gas diffusion, which has a very strong influence on the carbonation profile. Also, one can see that after 60 days, with a reduced CO_2 partial pressure, the carbonation effect is very limited and is close to the one obtained for a higher initial water content.

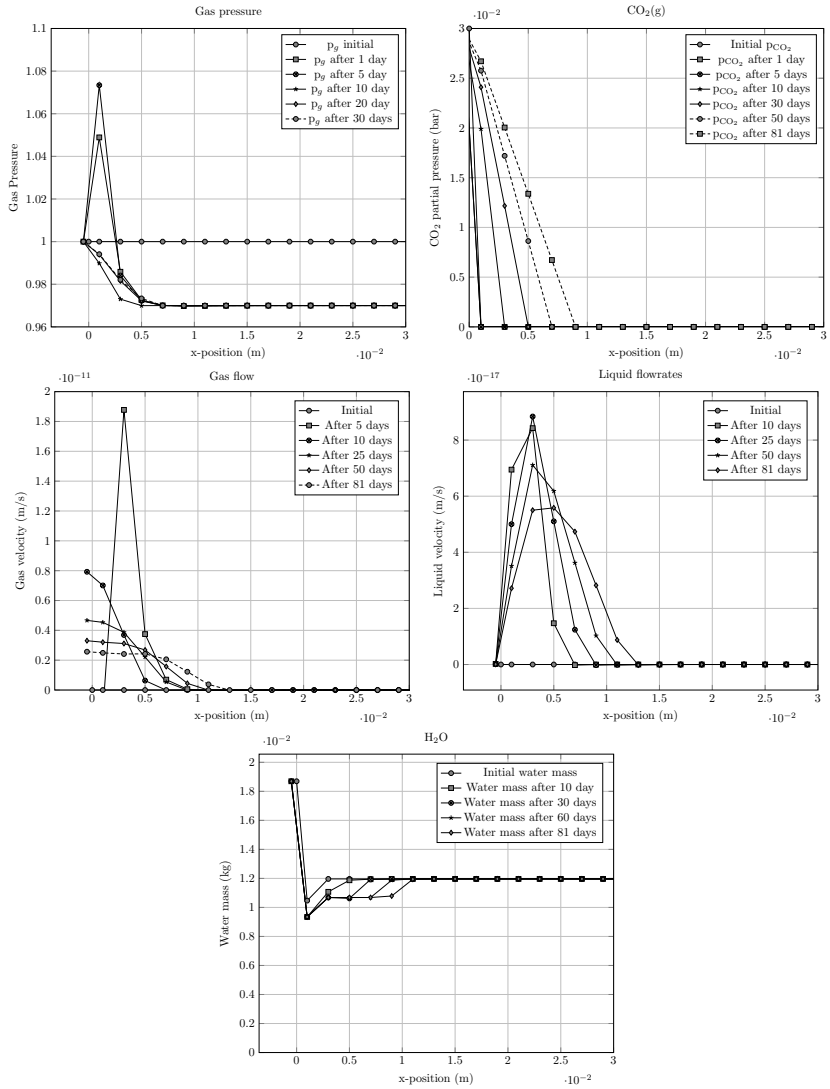

Figure 5: Evolution of gas and liquid flow parameters during the accelerated carbonation.

Regarding aqueous diffusion, sensitivity analysis indicated that its value does not play a significant role in the carbonation extent, as the dissolution precipitation reaction mainly depend on the gas diffusion. This does neither indicate that aqueous diffusion does not significantly evolve during these reactions or that the importance of this parameter can be discarded. Indeed, for higher liquid saturation, the diffusion in the gas phase might be significantly reduced, to the point where the gas phase could become disconnected. If such a situation occurs, diffusion in the aqueous phase should be assessed accurately.

From these results, we can conclude that moisture conditions play a major role for the

durability of these materials, because they strongly influence the gas diffusion, which is the main driver of the carbonation process. To be able to say that the presented behavior is physically representative, one needs to assess the validity of the used parameters in the Millington-Quirk relation, and actually measure the gas diffusion coefficient for different saturation.

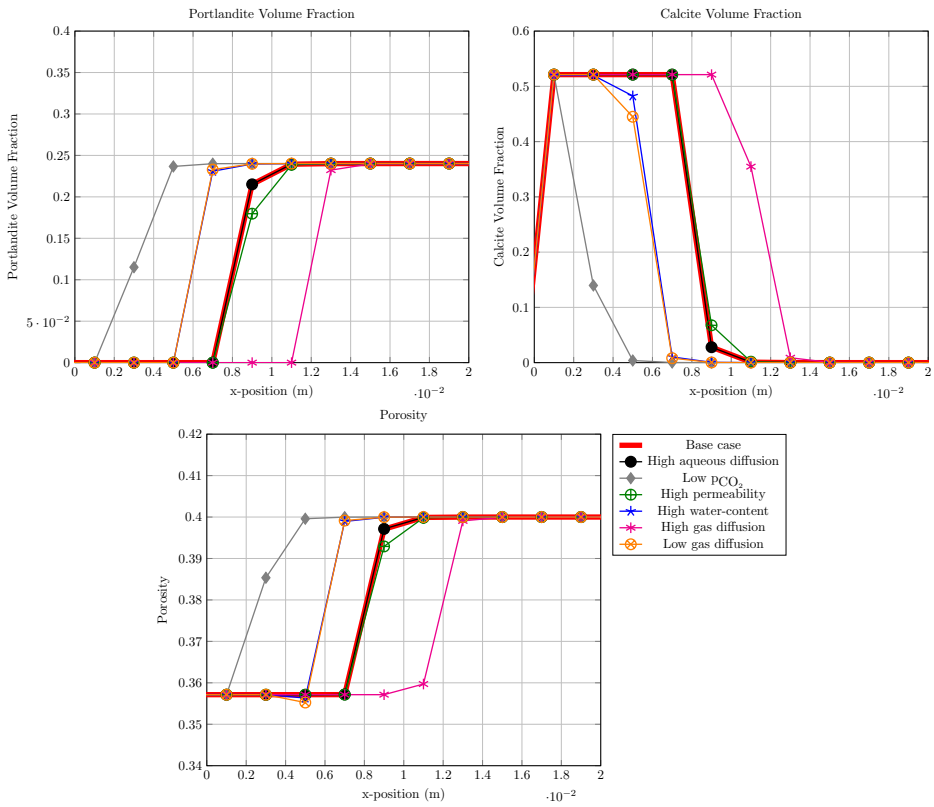

Figure 6: Sensitivity analysis. Comparison between the portlandite, calcite and porosity profiles after 60 days

3.3.3. Natural carbonation

Results of simulations of carbonation at natural and intermediate p_{CO_2} are given in figure 7. One can see that, after 300 days of simulation the first milimiter of cement is only depleted by 20% of portlandite for the natural carbonation. This simulation predicts that it would take 5 years before completely depleting portlandite in the first millimeter of cement. When p_{CO_2} is increased by a factor 10 (right of figure 7), one can notice that carbonation is accelerated by the same factor.

3.4. Results of the low-pH formulation

The same method was applied for the low pH formulation. The initial conditions were slightly changed to model the carbonation of the low-pH material: a higher poros-

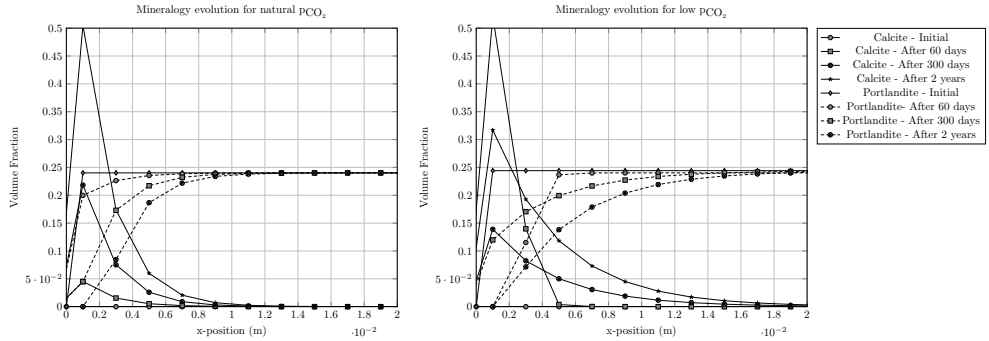

Figure 7: Comparison of portlandite and calcite profiles for the simulation of natural and intermediate p_{CO_2}

ity (55%) and similar initial saturation. Initial aqueous concentrations calculated at equilibrium with CSH(1.6) were given in table 6.

As the initial porosity and pore structure of this material is different, it is likely that its transport properties are different. However, to allow a more significant comparison with the results of the C_3S pastes, initial transport parameters were set so that initial effective diffusion coefficients are the same for both phase. However, one should measure the gas and transport properties of such a low-pH paste to obtain a simulation which is physically representative.

Results for the low-pH formulation are given in figure 8. One can see an increase in the carbonation extents and that the decalcification process is strongly accelerated and quickly involves important carbonation depths. After 40 days, the first 15mm of the material have been carbonated. It only requires two days to turn the first two millimeters into a silica gel (compared to 8 days for the C_3S paste). After 71 days, the carbonated depth is around 2cm, which is pretty close to the measured value. This seems to indicate that the effective gas diffusion coefficient is similar for the two investigated materials. However, the fracturing of the material is not modelled, neither is its impact on the transport properties.

3.5. Modelling conclusions

The presented modelling approach and results demonstrate that reactive transport modelling can be used to estimate the different coupled physico-chemical processes involved in the atmospheric carbonation of cementitious materials. However, an accurate model predicition heavily relies on the input parameters used to describe the materials. In particular, all the empirical relationships used in this model (Millington-Quirk for diffusion, van Genuchten relationships for the two-phase flow) need to be representative of the material.

Compared to experimentally measured parameters, the effective gas diffusion coefficient had to be increased (from 1-1.5 to 2.25 *times* 10^{-7} $m^2.s^{-1}$). This artificial increase in the effective gas diffusion coefficient could only be attributed to the appearance of cracks in the carbonated zone. Apart from this notable exception, it is important to realize that every parameter used to feed these empirical relationships were based on

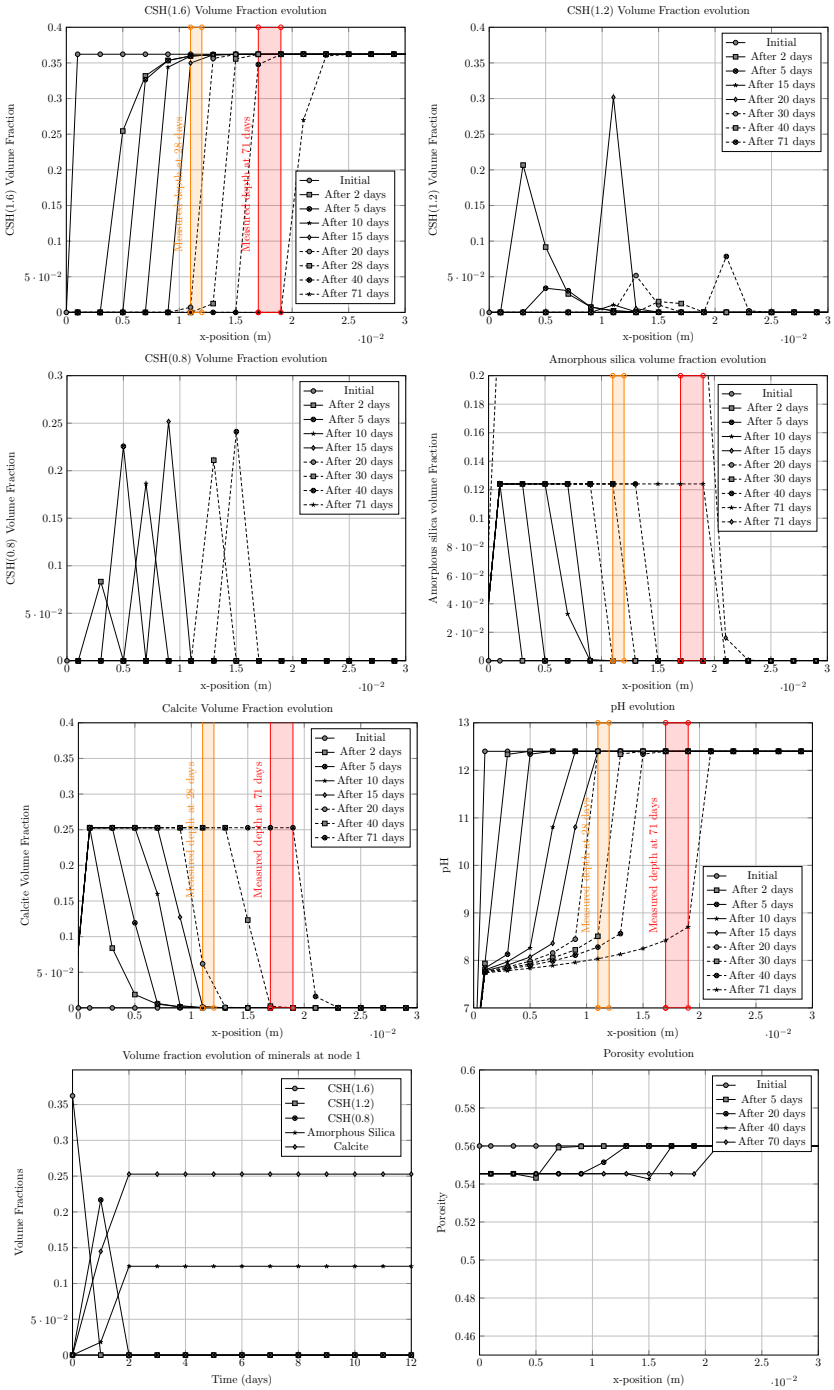

Figure 8: Evolution of the mineralogical and pH profiles during the accelerated carbonation of the low-pH paste. Measured carbonation dephs after 28 and 71 days (given in table 2) are highlighted in orange and red.

experimental and literature data, and led to an excellent comparison with measured carbonation depths.

However, important uncertainties remain on the use of these parameters particularly over an evolving pore structure. It is very likely that these laws are not suited to accurately represent the physical evolution of the material, and none of these parameters should be used lightly or extrapolated to any other situations. Indeed, [12] showed the importance of the Millington-Quirk parameters parameters when modelling simulation of drying and carbonation of cement materials. However, here, these parameters show minor importance, as the evolution of the porosity and saturation are not significant compared to drying situations. However, in the presented simulations, one could argue that the values attributed to these parameters are realistic.

Even though reactive transport modelling is able to describe these coupled phenomena, it is also clear that the use of reactive transport in cases of important mechanical coupling is far from being achieved: *e.g.* fracturation is bound to have a major impact on both diffusion and advection of gas. Hence, the application of reactive transport modelling on low-pH cement is probably not yet reasonable for a predictive purpose. Nevertheless, reactive transport modelling can help understanding what leads to mechanical damage, and therefore allow a predictive capability to assess for a potential damage. In other words, if mechanical models of the C-S-H structure provide, for example, a threshold decalcification (or shrinkage) rate above which fracturing is likely to occur, reactive transport modelling can investigate several cases and assess in which conditions mechanical integrity can be maintained.

4. Discussion

4.1. Validity of the reactive transport simulation

In the previous section, it was demonstrated that the presented mathematical formulation was suited to model the atmospheric carbonation of cementitious materials.

In order to be able to simulate the fate of different cement formulation, a detailed coupling with a mechanical model should be considered. Unfortunately, a full THCM coupling is not yet available to fully understand and predict the mechanical behavior of these materials under these conditions.

However, experimental results have shown a discrepancy in the mechanical responses of similar cementitious materials in similar conditions, *i.e.* an enriched CO_2 atmosphere. Let us focus briefly on the difference between the hydrated C_3S paste and the low-pH paste. The second material only differs from the C_3S paste by the fact that silica was added during the manufacturing to obtain pozzolonic reactions which consume portlandite, decrease pH and generate more C-S-H. This reaction tends to increase the overall porosity while shifting towards lower pore size. In this study, these two materials were cast, treated, cured and carbonated in very similar conditions, but exhibited very different mechanical responses to a similar geochemical perturbation. So how can one explain such discrepancies?

4.2. Scenario to account for differences of mechanical behavior

To try to understand this difference, let us describe what is likely responsible for the induced mechanical stresses during the carbonation process. In the described system, the

gas pressure is relatively low (atmospheric pressure) and approximately uniform through time in the system, *i.e.* the potential evolution of the gas-pressure due to the solid and water reactions is limited (did not exceed 10% increase, as shown in figure 5), and is compensated by advective fluxes. It is therefore likely that the induced stress finds its root in the evolution of the solid and liquid phase, rather than in the gas phase.

For both systems, calcite (and polymorphs) production depends both on the dissolution of CO_2(g) and the concentration and supply of calcium in the porewater. One could expect that, for low pH systems, the decreased concentration of calcium in the porewater would limit calcite (and other calcium carbonates) precipitation rate and therefore decrease the potential induced stresses in system. However, experimental results seem to contradict the latter conclusion. From this, we can assume that, up to a certain extent, calcite precipitation rate, which is mostly controled by the CO_2 partial pressure (and, to a lesser extent, surface area, the calcium concentration and the mineralogy), or the aqueous geochemistry in general, is not responsible for the induced stress.

For the hydrated C_3S paste, the different contributions to mechanical stresses are the increase/decrease of porosity induced by portlandite dissolution and calcite precipitation. Also, the dissolution of portlandite is accompanied by a release of water. As the molar volume of portlandite is slightly smaller than the one of calcite (33.1 vs 36.9 $cm^3.mol^{-1}$), there is a slight reduction of porosity. This total porosity evolution likely does not lead to a significant stress. Let us note, however, that in some cases ([45]) precipitation of secondary phases has a higher mechanical impact than the dissolution of the initial solid structure.

Furthermore, as portlandite dissolves, it usually leads to the formation of micrometric macropores, leaving room for calcite to precipitate. Also, because of the high cristallization pressures [26, 27] and solubilities [25] within the small pores, it is likely that calcite will precipitate in the larger pores.

For the low-pH cement pastes however, portlandite is not present and the C-S-H phase constitutes the solid structure of the paste. This has three main consequences. First, the porosity of these pastes generally consists in smaller pores (see figure 1). Second, calcite precipitation induces a sink term for the calcium concentration which induces a coupled decalcification and shrinkage of the C-S-H phase. Here, that shrinkage is coupled to a local additional stress induced by the precipitation of calcite. As the latter occurs within smaller pores (compared to C_3S paste) and that no micrometric pores are created from the dissolution of portlandite, the induced stresses are relatively more important. Three, the rate of the C-S-H decalcification is relatively larger than for the ordinary pastes. Indeed, the local calcium production in the porewater from local portlandite dissolution, or by diffusion from the sound areas of the cement are two mechanisms which limit the local rate at which the C-S-H decalcification occurs.

These three consequences imply that, for the low-pH pastes, the precipitation of calcite induce larger mechanical stress, faster and broader C-S-H decalcification, hence shrinkage. These can explain the higher crack density observed in figure 2. The decalcification rate was also understood as one of the main control on shrinkage kinetics in [62].

For the modelling perspective, the computation of the induced mechanical stresses linked to calcite precipitation would require a coupled pore-scale mechanical approach, not yet available. However, simulations of the low-pH paste (see figure 8) are able to reproduce the fast decalcification of the C-S-H. If dedicated experiments were able

to provide a decalcification rate above which C-S-H shrinkage would crack, reactive transport simulations could be used to determine if and when, severe mechanical damage could be expected.

If this process-based explanation is true, it indicates that the presence of portlandite inherently improves the mechanical robustness of a cementitious material in carbonating conditions, through a an additional buffer capacity. We use the "buffer" terminology because, as portlandite maintains pH while it is present, portlandite remains a calcium source which reduces the rate of C-S-H decalcification. So, as low-pH materials are considered for many engineering purposes for which their long-term mechanical stabilities have to be assessed, there is a need to confirm or refute this.

4.3. Experiments proposal

The previous considerations yield that a synthetic C-S-H gel would fracture under carbonation experiments. A way of investigating this effect would be to synthesise various similar C-S-H pastes with different porosities - densities, *i.e.* with a lower/higher water to solid ratios. As they all consist of a C-S-H structure, the pore structure would be similar between the different samples, except for the large pores, which would be in higher quantity for the high-porosity pastes. Therefore, the ones with the higher water contents / porosities (and lower densities) should have an easier time to accomodate the pressure increase. Hence, if these materials exhibit a similar crack density, this would indicate that C-S-H shrinkage is the main contributor to cracking, and that portlandite presence would only improve the mechanical robustness of these materials.

Another possibility would be to compare the responses between different materials with varying portlandite contents (achieved by adding a varying amount of silica to the mix). If true, the materials which contain the less portlandite should exhibit higher crack density.

5. Conclusion and perspectives

This paper focused on modelling the atmospheric carbonation of two cement materials, one being a hydrated C_3S paste, while the other represents a low-pH paste without portlandite. The modelling considers most of the relevant known physicochemical processes: two-phase compressible flow, gas and aqueous transport, solid-liquid-gas chemical equilibrium, including water production/consumption through chemical reactions and porosity changes. Furthermore, the coupling between these processes (generated fluid flow induced by mineral reactions) was considered and accurately modelled. The different input parameters required to model the atmospheric carbonation of the C_3S paste were directly measured on this specific material and commonly accepted values for empirical relationships were used (Millington-Quirk, unsaturated laws). A good agreement between simulated and measured carbonation depths was obtained, without the need of any fitting parameter. A sensitivity analysis was also performed which showed the influence of the different input parameters. This sensitivity analysis demonstrated that, under these conditions, gaseous diffusion unsurprisingly seemed to be the most influencial parameter.

While the validity of some of the used empirical parameters (two-phase flow, Millington-Quirk powers) should be questioned, we can assume that this mechanistic modelling approach is representative and extrapolable to other materials or carbonation conditions.

Moreover, good comparison between simulated and experimental carbonation depths were also found for the low-pH material. However, higher uncertainties regarding the representativity of the latter simulation exist. First, because the witnessed cracking was not taken into account. Second, because its diffusive transport properties were assumed the same as for the C_3S paste.

Also, it was observed experimentally in this study (and others), that low-pH materials exhibit a higher tendency to develop cracks during the carbonation. An accurate simulation would require two improvements.

First, it requires the ability to predict when and when fractures appear and being able to represent the evolution of the material's properties when fractures appear. Second, it requires to be able to understand whether or not, and when, fractures appear. While the first requirement might not be so complicated to model through the use of empirical relationships, the second one is harder to meet. As these two materials only differ in their pore size distributions, total porosity, and their portlandite content, only a pore-scale mechanistic approach could lead to a significant simulation of the considered phenomena.

The fact that the models managed to reproduce observed carbonation depths using constrained measured parameters without considering the impact of fractures is a good indication that reactive transport modelling can be used as a predictive tool for these reactions. As was stated above, uncertainties regarding the low-pH pastes persist. Further research should be dedicated to a thorough tracking of the carbonation depth, with C/S profiles, to be able to provide an understanding of how the diffusive transport properties of the material evolve, parallel to a chacarterization of the evolving crack-network.

A mechanistic explanation of the higher-observed crack developements of low-pH pastes was provided. In low-pH cements, the coupled effects of calcite precipitation in smaller pores, combined with a faster and broader C-S-H shrinkage due to the absence of portlandite seem to be responsible of the observed higher mechanical response. This indicates that reactive transport modelling on the REV scale will be tricky for the unique material which is cement. Indeed, the wide distribution of pore sizes and their connectivities (and their respective saturation state in unsaturated cases) seem to be responsible for the ability of a material to accomodate stresses. This suggests again that, for a continuum approach to be valuable or representative of an actual physical reality, the pore-scale effects need to be taken into account accurately. To that end, cementitious materials still constitute a challenge for the modelling perspective.

[1] Martin, G. R. (1986). A method for determining the relative permeability of concrete using gas. Magazine of Concrete Research, 38(135), 90-94.

[2] Dewaele, P. J., Reardon, E. J., and Dayal, R. (1991). Permeability and porosity changes associated with cement grout carbonation. Cement and concrete research, 21(4), 441-454.

[3] Claisse, P. A., El-Sayad, H. I., and Shaaban, I. G. (1999). Permeability and pore volume of carbonated concrete. Materials Journal, 96(3), 378-381.

[4] Ngala, V. T., and Page, C. L. (1997). Effects of carbonation on pore structure and diffusional properties of hydrated cement pastes. Cement and Concrete Research, 27(7), 995-1007.

[5] Litvan, G. G., and Meyer, A. (1986). Carbonation of granulated blast furnace slag cement concrete during twenty years of field exposure. Special Publication, 91, 1445-1462.

[6] Verbeck, G. (1958). Carbonation of hydrated Portland cement. In Cement and Concrete. ASTM International.

[7] Houst, Y. F. (1997). Carbonation shrinkage of hydrated cement paste. In Proc. 4th CANMET/ACI International Conference on Durability of Concrete (No. LTP-CONF-1997-005, pp. 481-491). CANMET, Ottawa, Canada.

[8] Houst, Y. F., and Wittmann, F. H. (2002). Depth profiles of carbonates formed during natural carbonation. Cement and concrete research, 32(12), 1923-1930.

[9] Borges, P. H., Costa, J. O., Milestone, N. B., Lynsdale, C. J., and Streatfield, R. E. (2010). Carbonation of CH and CSH in composite cement pastes containing high amounts of BFS. Cement and Concrete Research, 40(2), 284-292.
[10] Kutchko, B. G., Strazisar, B. R., Dzombak, D. A., Lowry, G. V., and Thaulow, N. (2007). Degradation of well cement by CO2 under geologic sequestration conditions. Environmental science and technology, 41(13), 4787-4792.
[11] Kamimura, K., Sereda, P. J., and Swenson, E. G. (1965). Changes in weight and dimensions in the drying and carbonation of Portland cement mortars. Magazine of Concrete Research, 17(50), 5-14.
[12] Georget, F., Prevost, J.H. and Huet, B. (2018). Impact of the microstructure model on coupled simulation of drying and accelerated carbonation. Cement and concrete research, 104, 1-12.
[13] Bary, B. and Sellier, A. (2004). Coupled moisture-carbon dioxide- calcium transfer model for carbonation of concrete. Cement and Concrete Research, 34, 1859-1872.
[14] Zha, X., Yu, M., Ye, J., and Feng, G. (2015). Numerical modeling of supercritical carbonatoin process in cement-based materials. Cement and Concrete Research, 72, 10-20.
[15] Wu, B. and Ye, G. (2017). Development of porosity of cement paste blended with supplementary cementitious materials after carbonation. Construction and Building Materials, 145. 52-61
[16] Zhang, Q. (2016). Mathematical modeling and numerical study of carbonation in porous concrete materials. Applied Mathematics and Computation, 281, 16-27.
[17] Glasser, F. P. (1999). Long-term leaching mechanisms of Portland cement-stabilized municipal solid waste fly ash in carbonated water. Cement and Concrete Research, 29(2), 179-186.
[18] Duguid, A., and Scherer, G. W. (2010). Degradation of oilwell cement due to exposure to carbonated brine. International Journal of Greenhouse Gas Control, 4(3), 546-560.
[19] Seigneur, N., Dauzères, A., Voutilainen, M., Detilleux, V., Labeau, P. E., and Dubus, A. (2017). Numerical representative elementary volume generation of a simplified cement paste and estimation of its diffusivity and comparison with dedicated experiments. Journal of Porous Media, 20(1).
[20] Morandeau, A., Thiery, M. and Dangla, P. (2014). Investigation of the carbonation mechanism of CH and CSH in terms of kinetics, microstructure, changes and moisture properties. Cement and Concrete Research, 56, 153-170.
[21] Jacquemet, N., Pironon, J., Lagneau, V., and Saint-Marc, J. (2012). Armouring of well cement in H2SCO2 saturated brine by calcite coatingExperiments and numerical modelling. Applied geochemistry, 27(3), 782-795.
[22] Šavija, B., and Luković, M. (2016). Carbonation of cement paste: understanding, challenges, and opportunities. Construction and Building Materials, 117, 285-301.
[23] Bildstein, O., Kervévan, C., Lagneau, V., Delaplace, P., Crédoz, A., Audigane, P., and Jullien, M. (2010). Integrative modeling of caprock integrity in the context of CO2 storage: evolution of transport and geochemical properties and impact on performance and safety assessment. Oil and Gas Science and TechnologyRevue de lInstitut Français du Pétrole, 65(3), 485-502.
[24] Jacquemet, N. (2006). Durabilité des matériaux de puits pétroliers dans le cadre d'une séquestration géologique de dioxyde de carbone et d'hydrogène sulfuré (Doctoral dissertation, Université Henri Poincaré-Nancy I).
[25] Emmanuel, S., and Berkowitz, B. (2007). Effects of poresize controlled solubility on reactive transport in heterogeneous rock. Geophysical Research Letters, 34(6).
[26] Osselin, F., Fen-Chong, T., Fabbri, A., Lassin, A., Pereira, J. M., and Dangla, P. (2013). Dependence on injection temperature and on aquifers petrophysical properties of the local stress applying on the pore wall of a crystallized pore in the context of CO2 storage in deep saline aquifers. The European Physical Journal Applied Physics, 64(2), 21101.
[27] Osselin, F., Fabbri, A., Fen-Chong, T., Dangla, P., Pereira, J. M., and Lassin, A. (2014). Stress from NaCl crystallisation by carbon dioxide injection in aquifers. Environmental Geotechnics, 2(5), 280-291.
[28] Dauzères, A. (2010). Etude expérimentale et modélisation des mécanismes physico-chimiques des interactions béton-argile dans le contexte du stockage géologique des déchets radioactifs (Doctoral dissertation, Poitiers).
[29] Wu, B., and Ye, G. (2017). Development of porosity of cement paste blended with supplementary cementitious materials after carbonation. Construction and Building Materials, 145, 52-61.
[30] Seigneur, N., Lagneau, V., Corvisier, J., and Dauzères, A. (2018). Recoupling flow and chemistry in variably saturated reactive transport modelling-An algorithm to accurately couple the feedback of chemistry on water consumption, variable porosity and flow. Advances in Water Resources, 122, 355-366.
[31] Namoulniara, K., Turcry, P., and Ait-Mokhtar, A. (2016). Measurement of CO2 effective diffusion

coefficient of cementitious materials. European Journal of Environmental and Civil Engineering, 20(10), 1183-1196.
[32] Groves, G.W., Rodway, D.I. and Richardson, I.G. (1990). The carbonation of hardened cement pastes. Advances in Cement research, 3(11), 117-125.
[33] Groves, G. W., Brough, A., Richardson, I.G., and Dobson, C.M. (1991). Progressive changes in the structure of hardened C3S cement pastes due to carbonation. Journal of the American Ceramic Society, 74(11), 2891,2896.
[34] Cui, H., Tang, W., Liu, W., Dong, Z. and Xing, F. (2015). Experimental study on effects of CO2 concentrations on concrete carbonation and diffusion mechanisms. Construction and Building Materials, 93, 522-527.
[35] Castellote, M., Fernandez, L., Andrade, C. and Alonso, C. (2009). Chemical changes and phase analysis of OPC pastes carbonated at different CO2 concentrations. Materials and Structures, 42(4), 515-525.
[36] Leemann, A., and Moro, F. (2017). Carbonation of concrete: the role of CO2 concentration, relative humidity and CO2 buffer capacity. Materials and Structures, 50(1), 30.
[37] Leemann, A., Nygaard, P., Kaufmann, J., and Loser, R. (2015). Relation between carbonation resistance, mix design and exposure of mortar and concrete. Cement and Concrete Composites, 62, 33-43.
[38] Auroy, M., Poyet, S., Le Bescop, P., Torrenti, J. M., Charpentier, T., Moskura, M., and Bourbon, X. (2018). Comparison between natural and accelerated carbonation (3% CO 2): Impact on mineralogy, microstructure, water retention and cracking. Cement and Concrete Research, 109, 64-80.
[39] Cole, W. F., and Kroone, B. (1959). Carbonate minerals in hydrated portland cement. Nature, 184(4688), BA-57.
[40] Auroy, M., Poyet, S., Le Bescop, P., Torrenti, J. M., Charpentier, T., Moskura, M., and Bourbon, X. (2015). Impact of carbonation on unsaturated water transport properties of cement-based materials. Cement and Concrete Research, 74, 44-58.
[41] Auroy, M. (2014). Impact de la carbonatation sur les propriétés de transport d'eau des matériaux cimentaires. Thèse de doctorat de l'université Paris-Est.
[42] Sin, I., Lagneau, V., Corvisier, J. Integrating a compressible multicomponent two-phase flow into an existing reactive transport simulator (2017) Advances in Water Resources, 100, pp. 1339-1351.
[43] Marsily, G. d., 1981. Hydrologie quantitative. Masson, Paris
[44] Lagneau, V., van der Lee, J. HYTEC results of the MoMas reactive transport benchmark. (2010) Computational Goesciences, 14, pp. 435-449
[45] Planel, D. (2002). Les effets couplés de la précipitation d'espèces secondaires sur le comportement mécanique et la dégradation chimique des bétons (Doctoral dissertation, Université de Marne-la-Vallée).
[46] Lagneau, V., van der Lee, J. Operator-splitting-based reactive transport models in strong feedback of porosity change: The contribution of analytical solutions for accuracy validation and estimator improvement. (2010) J. Contam. Hydrol. 112(1), 118-129
[47] van der Lee, J., de Windt, L., Lagneau, V., Goblet, P. Module-oriented modelling of reactive transport with HYTEC. (2003). Computational Geosciences. 29(3), 265-275.
[48] Van Der Lee, J., De Windt, L., Lagneau, V., and Goblet, P. (2002). Presentation and application of the reactive transport code HYTEC. In Developments in Water Science (Vol. 47, pp. 599-606). Elsevier.
[49] Lichtner, P. Continuum formulation of multicomponent-multiphase reactive transport. (1996). Rev. Mineral. 34: Reactive Transport in Porous Media, 1-81
[50] Millington, R., Quirk, J. Permeability of porous solids. (1961) Trans. Faraday Soc. 57, 1200-1207.
[51] Pitzer,K. Ion interaction approach: theroy and data correlation. (1991) Activity Coeff. Electrolyte Solut. 2, 75-153
[52] Archie, G.E. et al. The electrical resistivity log as an aid in determining some reservoir characteristics. (1942). Transactions of the AIME, vol 146, no 01, 54-62.
[53] Regnault, O., Lagneau, V., and Schneider, H. (2009). Experimental measurement of portlandite carbonation kinetics with supercritical CO2. Chemical Geology, 265(1-2), 113-121.
[54] Monteiro, I., Branco, F. A., De Brito, J., and Neves, R. (2012). Statistical analysis of the carbonation coefficient in open air concrete structures. Construction and Building Materials, 29, 263-269.
[55] Silva, A., Neves, R., and De Brito, J. (2014). Statistical modelling of carbonation in reinforced concrete. Cement and Concrete Composites, 50, 73-81.
[56] Morel, F., Hering, J. Principles and applications of Aquatic chemistry. (1993). John Wiley & Sons, New York.

[57] de Windt, L., Devillers, P. Modeling the degradation of Portland cement pastes by biogenic organic acids. Cement and Concrete Research, 2010, vol. 40, no 8, p. 1165-1174.
[58] Corvisier, J., Bonvalot, A-F., Lagneau, V. et al. Impact of co-injected gases on CO2 storage sites: Geochemical modeling of experimental results. Energy Procedia, 2013, vol. 37, p. 3699-3710.
[59] Groves, G. W., Brough, A., Richardson, I. G., and Dobson, C. M. (1991). Progressive changes in the structure of hardened C3S cement pastes due to carbonation. Journal of the American Ceramic Society, 74(11), 2891-2896.
[60] Thouvenot, P., Bildstein, O., Munier, I., Cochepin, B., Poyet, S., Bourbon, X., and Treille, E. (2013). Modeling of concrete carbonation in deep geological disposal of intermediate level waste. In EPJ Web of Conferences (Vol. 56, p. 05004). EDP Sciences.
[61] Sin, I. Numerical simulation of compressible two-phase flow and reactive transport in porous media-Applications to the study of CO2 storage and natural gas reservoir. 2015. Thèse de doctorat. École Nationale Supérieure des Mines de Paris.
[62] Kumarappa, D. B., Peethamparan, S., and Ngami, M. (2018). Autogenous shrinkage of alkali activated slag mortars: Basic mechanisms and mitigation methods. Cement and Concrete Research, 109, 1-9.
[63] Wan, K., Xu, Q., Wang, Y., and Pan, G. (2014). 3D spatial distribution of the calcium carbonate caused by carbonation of cement paste. Cement and Concrete Composites, 45, 255-263.
[64] Van Genuchten, M. T., Nielsen, D. R. (1985). On describing and predicting the hydraulic properties. In Annales Geophysicae (Vol. 3, No. 5, pp. 615-628).
[65] Carrayrou, J., Hoffmann, J., Knabner, P., Krutle, S., De Dieuleveult, C., Erhel, J. and Macquarrie, K. T. (2010). Comparison of numerical methods for simulating strongly nonlinear and heterogeneous reactive transport problems - the MoMaS benchmark case. Computational Geosciences, 14(3), 483-502.
[66] Seigneur, N., Dauzères, A., Sammaljärvi, J., Voutilainen, M., Labeau, P. E., Dubus, A., and Detilleux, V. (2017). Transport properties evolution of cement model system under degradation-Incorporation of a pore-scale approach into reactive transport modelling. Physics and Chemistry of the Earth, Parts A/B/C, 99, 95-109.
[67] Seigneur, N., Mayer, K.U., Steefel, C.I. (2019). Reactive Transport in Evolving Porous Media. Reviews in Mineralogy and Geochemistry 85: 197-238.
[68] Helgeson, H. C., Kirkham, D. H., and Flowers, G. C. (1981). Theoretical prediction of the thermodynamic behavior of aqueous electrolytes by high pressures and temperatures; IV, Calculation of activity coefficients, osmotic coefficients, and apparent molal and standard and relative partial molal properties to 600 degrees C and 5kb. American journal of science, 281(10), 1249-1516.
[69] Helgeson, H. C. (1969). Thermodynamics of hydrothermal systems at elevated temperatures and pressures. American journal of science, 267(7), 729-804.
[70] Kangni-Foli, E., Poyet, S., Le Bescop, P., Dauzères, A., L'Hôpital, E., Charpentier, T., d'Espinose de Lacaillerie, J.-B.. Designing a model system for Low-pH cement, Proceedings of Symposium NUWCEM, Avignon, France, Oct. 2018.
[71] Kangni-Foli, E., Poyet, S., Le Bescop, P., Dauzères, A., L'Hôpital, E., Charpentier, T., d'Espinose de Lacaillerie, J.-B.. Designing a model system for Low-pH cement, Proceedings of SMSS conference, Rovinj, Croatia, March 2019.
[72] Rimmelé, G., Barlet-Gouédard, V., Porcherie, O., Goffé, B., and Brunet, F. (2008). Heterogeneous porosity distribution in Portland cement exposed to CO2-rich fluids. Cement and Concrete Research, 38(8-9), 1038-1048.
[73] Houst, Y. F., and Wittmann, F. H. (1994). Influence of porosity and water content on the diffusivity of CO2 and O2 through hydrated cement paste. Cement and Concrete Research, 24(6), 1165-1176.
[74] Blanc, P., Lassin, A., Piantone, P., Azaroual, M., Jacquemet, N., Fabbri, A., and Gaucher, E. C. (2012). Thermoddem: A geochemical database focused on low temperature water/rock interactions and waste materials. Applied Geochemistry, 27(10), 2107-2116.
[75] Kangni-Foli, E., Poyet, S., Le Bescop, P., Charpentier T., Bernarchy-Barbé F., Dauzères, A., L'Hôpital, E., Neji M., d'Espinose de Lacaillerie, J.-B. Designing a model system for cementitious materials with variable calcium to silica ratio. Submitted to Cement and Concrete Composites.
[76] Jeen, S. W., Mayer, K. U., Gillham, R. W., and Blowes, D. W. (2007). Reactive transport modeling of trichloroethene treatment with declining reactivity of iron. Environmental science and technology, 41(4), 1432-1438.
[77] Daval, D., Martinez, I., Corvisier, J., Findling, N., Goff, B., and Guyot, F. (2009). Carbonation of Ca-bearing silicates, the case of wollastonite: Experimental investigations and kinetic modeling.

Chemical Geology, 265(1-2), 63-78.
[78] Harrison, A. L., Dipple, G. M., Power, I. M., and Mayer, K. U. (2016). The impact of evolving mineralwatergas interfacial areas on mineralfluid reaction rates in unsaturated porous media. Chemical Geology, 421, 65-80.